nature physics

ARTICLES

https://doi.org/10.1038/s41567-022-01672-2

Exact solutions for the wrinkle patterns of confined elastic shells

Ian Tobasco[1]✉, Yousra Timounay[2,3], Desislava Todorova[4], Graham C. Leggat[2], Joseph D. Paulsen[2,3]✉ and Eleni Katifori[4]✉

Complex textured surfaces occur in nature and industry, from fingerprints to lithography-based micropatterns. Wrinkling by confinement to an incompatible substrate is an attractive way of generating reconfigurable patterned topographies, but controlling the often asymmetric and apparently stochastic wrinkles that result remains an elusive goal. Here, we describe a new approach to understanding the wrinkles of confined elastic shells, using a Lagrange multiplier in place of stress. Our theory reveals a simple set of geometric rules predicting the emergence and layout of orderly wrinkles, and explaining a surprisingly generic co-existence of ordered and disordered wrinkle domains. The results agree with numerous test cases across simulation and experiment and represent an elementary geometric toolkit for designing complex wrinkle patterns.

Dried fruits wrinkle for the same reason that leaves and flowers do, namely mechanical instabilities arising from a mismatch in lengths[1–7]. A similar mismatch manifests when a thin elastic shell adheres to a substrate of a different shape[8–12]. Can such incompatibilities be used to design and control complex wrinkled surfaces at will? Wrinkles have been in the limelight for their theoretical importance in understanding geometric nonlinearities in elasticity[13–20] and also for their practical significance in emerging engineering applications such as lithography-free micropatterning[21–24]. Yet, despite decades of study, a general predictive theory of confinement-induced wrinkling remains elusive. Such a theory would enable the creation of targeted yet reconfigurable wrinkle patterns and could identify the broadest possible class of wrinkle morphologies that can be obtained through geometrically incompatible confinement.

Predicting the wrinkling of confined elastic shells is a difficult problem of nonlinear mechanics. Basic theoretical issues stem from a lack of applied tensile forces that would act to organize the response. In problems dominated by tension, the guiding principle is known as tension field theory[25–27], and solving it is the first step in the far-from-threshold expansion that has explained many tension-driven patterns[9,28–32]. Organized wrinkles nevertheless manifest in confined shells subject to weak or even zero tensile loads[8,16], raising the question of what sets their features. Although theoretical methods beyond tension field theory have been devised[19], their use requires advance knowledge of the wrinkled topography. Here, we show using theory, experiment and simulation that the wrinkles of confined shells are in fact predicted by a compact set of simple, geometric rules. We derive our rules using a stress-like Lagrange multiplier that arises from a maximum coverage problem for the macroscopic displacement of the shell (equation (3)).

These rules imply a string of predictions about the nature of confinement-driven wrinkling, which we confirm using experiments and simulations over a broad range of parameters and shell shapes. As we prove, a typical shell exhibits finitely many, ordered wrinkle domains where the wrinkle layout is robust. The theory also anticipates the existence of disordered wrinkle domains, whose local features behave stochastically but whose location is well defined (Fig. 1a,b). Second, the arrangement of these domains, and their division into ordered versus disordered, is fundamentally tied to the shell's medial axis, a distinguished locus of points from geometry. Third, although the wrinkle amplitude depends on the details of the shell's natural Gaussian curvature, within an ordered domain, the wrinkle topography actually depends only on its sign. Finally and perhaps most surprisingly, the wrinkle domains of oppositely curved shells are reciprocally related, so that the response of a given shell can be deduced from another. Although our study focuses on the model problem of a shallow shell confined to a plane, we imagine that a similar approach can be taken to understand confinement-driven patterns more generally, including ones arising from differential growth or in response to external stimuli[15,33,34]. We turn to introduce the setup of our study and to state our rules.

Confined shells. A prototypical setup for confinement-driven wrinkling is shown in Fig. 1a,b, where square domains are cut out from a thin saddle shell or spherical cap and are confined to an initially planar liquid bath. By Gauss's theorema egregium, no length-preserving map exists from a curved surface to the plane. Here, this geometric incompatibility manifests as a mechanical instability producing a wrinkle pattern. Figure 3 shows similar wrinkles obtained by altering the cutout shape from a square to a triangle, rectangle, ellipse or some other shape altogether. The layout of the resulting patterns depends strongly on the chosen cutout shape, as well as on the sign of the shell's initial Gaussian curvature κ, which is negative for saddle cutouts and positive for spherical ones. Complicating things further, the typical spherical shell exhibits a mixed 'ordered–disordered' response. In disordered regions, such as the central diamonds in Fig. 1b, the response is sensitive to perturbations and changes between trials. In ordered regions, the wrinkles are robust and repeatable.

To decipher this zoo of patterns, look first at the wrinkles of the saddle cutouts in Figs. 1–3 ($\kappa<0$). Apparently, their wrinkles fall along paths of quickest exit from the cut-out shape. Such paths are line segments that meet the boundary perpendicularly and meet

[1]Department of Mathematics, Statistics and Computer Science, University of Illinois at Chicago, Chicago, IL, USA. [2]Department of Physics, Syracuse University, Syracuse, NY, USA. [3]BioInspired Syracuse: Institute for Material and Living Systems, Syracuse University, Syracuse, NY, USA. [4]Department of Physics and Astronomy, University of Pennsylvania, Philadelphia, PA, USA. ✉e-mail: itobasco@uic.edu; jdpaulse@syr.edu; katifori@sas.upenn.edu

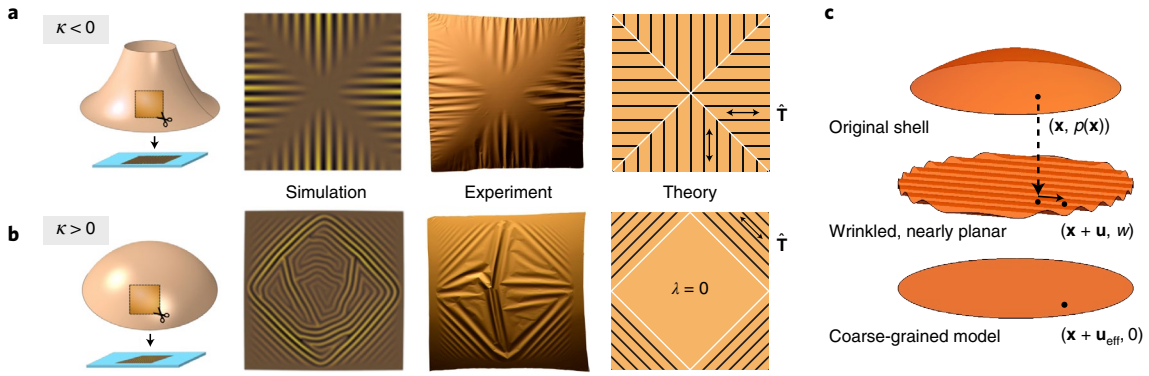

Fig. 1 | Wrinkling of confined shells. Wrinkle patterns result when initially curved shells are confined nearby a plane. **a**,**b**, Simulations and experiments of square cutouts from a saddle (**a**) and a sphere (**b**) show domains of robustly ordered wrinkles, alongside a more disorderly response in the spherical case (central diamonds in **b**). We present a coarse-grained theory to predict the type and layout of such wrinkle domains. **c**, Coarse-graining wrinkles. A point $(\mathbf{x}, p(\mathbf{x}))$ in the initial shell is displaced along the plane by $\mathbf{u}$ and out of the plane to a height w. The coarse-grained fields $\mathbf{u}_{\rm eff}$ and $w_{\rm eff}=0$ express a theoretical limit in which the shell is infinitesimally wrinkled and perfectly confined.

each other at the medial axis or skeleton of the shell, that is, the locus of points equidistant by closest approach to multiple boundary points (shown in white). Now look at the spherical cutouts ($\kappa>0$). Their wrinkles are also set by the medial axis, although this fact is not immediately clear. The key is Fig. 2, which reveals that the wrinkles of saddle and spherical shells come in reciprocal pairs. Most points **p** on the medial axis have exactly two closest boundary points, called **q** and **r** in Fig. 2b. While saddle cutouts wrinkle along the segments **pq** and **pr**, spherical cutouts wrinkle along the segment **qr**. Taken together, the ordered wrinkles of saddle and spherical shells form the legs of a special family of isosceles triangles whose layout is determined by the medial axis as shown.

Notably, the legs of these isosceles triangles do not always cover the entire shell. There can exist 'leftover' regions linked to exceptional points **p** on the medial axis with three or more closest boundary points. Figure 2e shows one such **p** and its four closest boundary points **q**, **r**, **s** and **t**. While **pq**, **pr**, **ps** and **pt** are along the ordered wrinkles of the saddle cutout, the polygon **qrst** supports disorder for its spherical twin. In general, the convex hull of three or more closest boundary points can support disorder in a spherical cutout. The possibility of infinitely many closest boundary points occurs for a spherical disc. It is totally disordered in our simulations and experiments, save for a small flattened rim[12].

These simple rules successfully capture wrinkle patterns across 111 experiments and several hundred more simulations. In the experiment, polystyrene films (Young's modulus $E=3.4\,\mathrm{GPa}$, Poisson's ratio $\nu=0.34$) of thickness $120\,\mathrm{nm}<t<430\,\mathrm{nm}$ are spin-coated on curved glass substrates. The spherical or saddle shape of the substrate imparts a finite rest curvature on the shell, with principal radii of curvature R ranging from 13 to 39 mm. Cutouts of width $2.5\,\mathrm{mm}<W<16\,\mathrm{mm}$ are released onto a flat water bath with surface tension $\gamma_{\rm lv}=0.072\,\mathrm{N\,m^{-1}}$ and gravitational stiffness $K=\rho g$. The experiments reside in the limit of weak tension $\gamma_{\rm lv}R^2\ll YW^2$, moderately stiff substrate $KW^2\gtrsim\gamma_{\rm lv}$ and small bending stiffness $BKR^4\ll Y^2W^4$, where $Y=Et$ and $B=Et^3/[12(1-\nu^2)]$ are the stretching and bending moduli. Being shallow yet much larger than the characteristic substrate-dominated wrinkle wavelength, $(B/K)^{1/4}\ll W\ll R$, the cutouts adopt approximately planar shapes and wrinkle as they float on the water bath (Figs. 1–3).

To probe the role of surface tension in setting the patterns, we perform ABAQUS simulations of shells on a liquid substrate in a similar parameter regime, but with the surface tension set to zero so that no forces are applied at the lateral shell boundary. The result

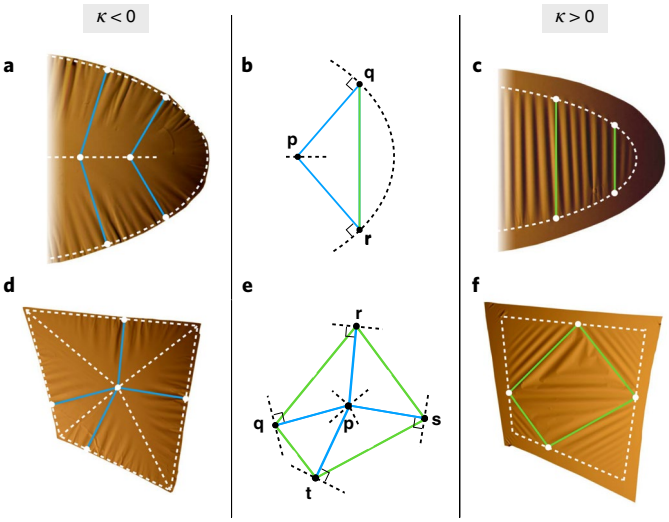

Fig. 2 | Simple rules for wrinkles. a–**c**, Ordered wrinkles in initially saddle and spherical shells (right halves of elliptical cutouts shown). Ordered wrinkles pair between shells to form a family of isosceles triangles (**b**) determined by the theory. For saddle shells (**a**), wrinkles follow the blue segments **pq** and **pr**. For spherical shells (**c**), they follow the green segment **qr**. The point **p** is on the medial axis, and **q** and **r** are its closest boundary points. **d**–**f**, Finding a disordered domain. In the given cutout shape, the point **p** has more than two closest boundary points (**q**, **r**, **s** and **t**) (**e**). For the saddle shell (**d**), ordered wrinkles follow the blue segments **pq**, **pr**, **ps** and **pt**. For the spherical shell (**f**), the green polygon **qrst** is disordered.

is a 'softly stamped' version of the well-known example of a plate pressed into a hard spherical mould[8,19]. Similar patterns arise in the simulation and the experiment, with the layout of the ordered domains and the location of the disordered domains being the same (Fig. 1a,b). The conclusion, which should be compared against the paradigm of tension as an organizing force determining wrinkle patterns[26,27], is that well-defined and spatially complex patterns persist even without applied tensile forces. Simulations of shells with nonconstant initial Gaussian curvatures $\kappa(\mathbf{x})$ reveal the even more curious fact that, as long as the initial Gaussian curvature of a shell

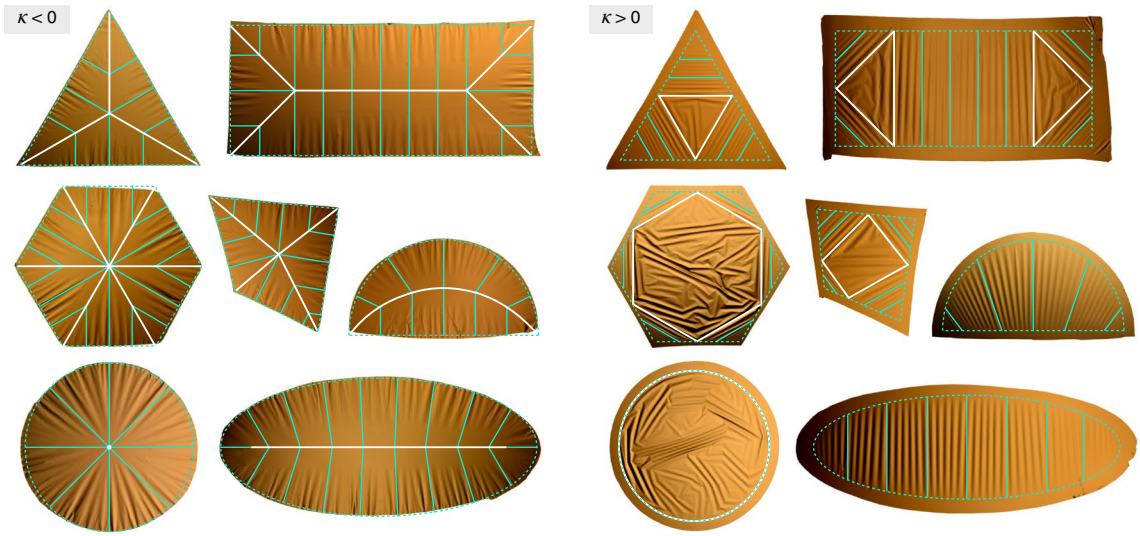

Fig. 3 | Floating shells. Solid cyan lines show the directions of the field $\hat{\mathbf{T}}$ determined by solving the coarse-grained theory, overlaid on floating shells arranged by the sign of their initial Gaussian curvature (saddle-shaped on the left, spherical on the right). Regions covered by these lines are predicted to be ordered ($\lambda > 0$ in the theory). Any disorder is predicted to occur in regions absent these lines (where $\lambda = 0$). For saddle shells, wrinkles decay towards the medial axis in white. For spherical shells, wrinkles decay towards the boundary. Dotted cyan curves show ideal shapes used in the predictions. Flattened regions are treated in the theory as infinitesimally fine. Experimental parameters are presented in Supplementary Tables S1 and S2.

is of one sign (either positive or negative everywhere), the patterns are the same as for shells with approximately constant curvature (compare Figs. 3 and 4).

Minimizing energy by maximizing coverage. We turn to explain these remarkably robust features of confinement-driven wrinkling and to derive our simple rules. We do so by analysing a novel coarse-grained model for incompatibly confined shallow shells from ref. [35], which we summarize now. Consider the setup in Fig. 1c, where a material point $(\mathbf{x}, p(\mathbf{x}))$ in the initial shell displaces to $(\mathbf{x}+\mathbf{u}(\mathbf{x}), w(\mathbf{x}))$ on the bath. The reference point $\mathbf{x} = (x_1, x_2)$ is in the shell's initial planform $\Omega \subset \mathbb{R}^2$, for example, a square in Fig. 1a,b. The displacements $\mathbf{u} = (u_1, u_2)$ and $w - p$ are respectively parallel and perpendicular to the initial bath. Patterns manifest through minimization of the system energy, $U = U_{\text{shell}} + U_{\text{subs}}$, where U_{shell} is the energy of bending and stretching the shell and U_{subs} is the gravitational potential energy of the bath plus its liquid surface energy (the latter being set to zero in the simulations)[3,36].

Energy minimizations of this type are usually solved via tension field theory[26,27], which involves an expansion about a uniaxially or biaxially tensile effective displacement $(\mathbf{u}_{\text{eff}}, -p)$. This effective state is obtained by coarse-graining away the wrinkles from the shell's physical displacement $(\mathbf{u}, w - p)$, in a limit where the wrinkle wavelength and amplitude go to zero (Fig. 1c). The typical explanation is that the direction of the wrinkles is set by tensile boundary loads, which stabilize their peaks and troughs. Yet, our patterns occur in confined shells subject to small or even zero boundary loads, suggesting an alternate expansion about a uniaxially or biaxially compressive state, that is, one that is tension free. To motivate this further, note that, in such a situation, one may expect the stretching energy of the shell to be subdominant to its bending and substrate energies[19]. Under a simplifying hypothesis guaranteeing this hierarchy, ref. [35] obtained an expansion of the system energy about a general tension-free state. As obtained, this expansion is outside the parameter range of the experiments and simulations. Nevertheless, for each $\mathbf{u}_{\text{eff}}$, the energy was found to be proportional to $\gamma_{\text{eff}} := \gamma_{\text{lv}} + 2\sqrt{BK}$ with $U/\gamma_{\text{eff}} = \int_\Omega \frac{1}{2}|\nabla w|^2 \, \mathrm{d}\mathbf{x}$ at leading order, up to a constant not depending on the effective state.

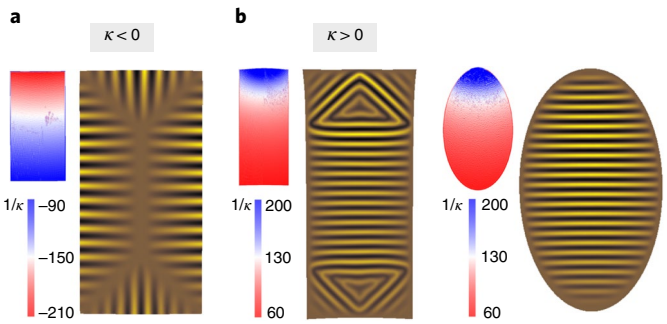

Fig. 4 | Variable-curvature shells. a,**b**, Simulations show initially negatively (**a**) or positively curved (**b**) shells confined nearby a plane. Colour maps show the inverse of the initial Gaussian curvature $\kappa(\mathbf{x})$. The patterns are independent of its precise values but depend strongly on its sign. The wrinkle amplitude reflects the curvature. Simulation parameters are presented in Supplementary Table S3.

To bring this into a more useful form, note that the strain $\varepsilon_{ij}(\mathbf{u}, w) = (\partial_i u_j + \partial_j u_i + \partial_i w \partial_j w - \partial_i p \partial_j p)/2$, $i, j \in \{1, 2\}$ tends to zero in the expansion, so that the shell's total area is asymptotically conserved:

$$\Delta A_{\text{tot}} = \int_\Omega \frac{1}{2}|\nabla p|^2 \, \mathrm{d}\mathbf{x} - \int_\Omega \nabla \cdot \mathbf{u} + \frac{1}{2}|\nabla w|^2 \, \mathrm{d}\mathbf{x} \to 0. \qquad (1)$$

Taking $\mathbf{u} \to \mathbf{u}_{\text{eff}}$ gives the following expression for the leading-order energy of a confined shallow shell[35]:

$$\frac{U}{\gamma_{\text{eff}}} \to \int_\Omega \frac{1}{2}|\nabla p|^2 \, \mathrm{d}\mathbf{x} - \int_{\partial\Omega} \mathbf{u}_{\text{eff}} \cdot \hat{\mathbf{n}} \, \mathrm{d}s := \Delta A\{\mathbf{u}_{\text{eff}}\}, \qquad (2)$$

where $\hat{\mathbf{n}}$ is the outwards-pointing unit normal to the boundary, $\partial\Omega$. This way of writing the energy emphasizes the role of the difference $\Delta A = A_{\text{init}} - A_{\text{eff}}$ between the shell's initial area $A_{\text{init}} = \int_\Omega 1 + \frac{1}{2}|\nabla p|^2 \, \mathrm{d}\mathbf{x}$ and the area covered by its infinitesimally wrinkled, perfectly planar limit, $A_{\text{eff}} = \int_\Omega 1 + \nabla \cdot \mathbf{u}_{\text{eff}} \, \mathrm{d}\mathbf{x}$.

This difference accounts for the area that is 'lost' asymptotically to wrinkles. It sets the energy of confinement per equation (2). Notably, this energy is not proportional to the stretching modulus Y because significant tension is not involved. Indeed, equation (2) was found to hold even in situations lacking boundary loads ($\gamma_{lv}=0$), in stark contrast to tension field theory. As we will show, the analysis of equation (2) leads to the patterns observed in our experiments and simulations, raising the question of whether it can be justified in a wider parameter range.

Optimizing the result of equation (2) determines the effective displacement of the shell. To help visualize this, imagine first projecting the shell directly into the plane, such that it is in a state of total compression. While this compression can be relieved by wrinkling, it can also be reduced by lateral displacements within the plane. These displacements take advantage of the liquid nature of the bath, which allows the shell to 'get out of its own way'. Their typical magnitude is $\sim W^3/R^2$, making them much larger than the wrinkles, whose lateral oscillations are $\sim(B/K)^{1/4}(W/R)^2$. The bulk lateral displacements are called $\mathbf{u}_{\rm eff}$ in the coarse-grained theory and are selected to minimize the cost of their accompanying wrinkles, captured by ΔA.

Importantly, this minimization is done under the constraint that $(\mathbf{u}_{\rm eff}-p)$ is tension free, to prevent the shell from stretching at a higher energy cost. To enforce this, we use the effective strain $(\varepsilon_{\rm eff})_{ij}(\mathbf{u}_{\rm eff}) := (\partial_i(\mathbf{u}_{\rm eff})_j + \partial_j(\mathbf{u}_{\rm eff})_i - \partial_i p\partial_j p)/2$ obtained by setting $\mathbf{u}=\mathbf{u}_{\rm eff}$ and $w=0$ into the previous formula for the strain of a shallow shell. While the physical strain ε tends to zero, the effective strain $\varepsilon_{\rm eff}$ is nonzero due to wrinkling. Its eigenvalues are constrained to be nonpositive, a situation we denote by $\varepsilon_{\rm eff}\leq 0$. As in tension field theory, a strictly negative eigenvalue indicates a length lost to wrinkles in the limit. A zero eigenvalue means that length is preserved. Thus, we arrive at the maximum coverage problem[35]

$$\min \Delta A\{\mathbf{u}_{\rm eff}\} \quad \text{subject to} \quad \varepsilon_{\rm eff}(\mathbf{u}_{\rm eff}) \leq 0. \tag{3}$$

By minimizing the area lost to infinitesimal wrinkles, the coarse-grained shell covers a maximal area in the plane. Using this attractive geometric variational principle, we shall deduce the phenomenology of wrinkle domains.

The locking stress Lagrange multiplier. To uncover the patterns predicted by the maximum coverage problem, we now introduce a notion of 'effective stress' to pair with the effective strain. Recognizing the nonholonomic nature of the constraint $\varepsilon_{\rm eff}\leq 0$, we replace it with a symmetric matrix-valued Lagrange multiplier field $\sigma_{\rm L}(\mathbf{x})$ that we call the locking stress (see Discussion for nomenclature). We require that $\sigma_{\rm L}\geq 0$, meaning that its eigenvalues are non-negative. We define the Lagrangian

$$\mathcal{L}\{\mathbf{u}_{\rm eff},\sigma_{\rm L}\} = \Delta A\{\mathbf{u}_{\rm eff}\} + \int_\Omega \sigma_{\rm L} : \varepsilon_{\rm eff}(\mathbf{u}_{\rm eff}) \tag{4}$$

for all $\mathbf{u}_{\rm eff}$ and $\sigma_{\rm L}\geq 0$ and seek a saddle point. Note that $\sigma_{\rm L} : \varepsilon_{\rm eff} = \Sigma_{i,j}(\sigma_{\rm L})_{ij}(\varepsilon_{\rm eff})_{ij}$. Enforcing stationarity of $\mathbf{u}_{\rm eff}$, we find that $\nabla\cdot\sigma_{\rm L}=0$ in the shell Ω and $\sigma_{\rm L}\hat{\mathbf{n}}=\hat{\mathbf{n}}$ at its boundary $\partial\Omega$. As discussed in Methods, a relaxation of the boundary conditions ensures the existence of a saddle point: we enforce them from the outside of the shell, but not necessarily from its inside. There, we also derive the orthogonality relation

$$\sigma_{\rm L} : \varepsilon_{\rm eff} = 0 \tag{5}$$

relating the locking stress to the effective strain. At this point, we have everything we need to solve for the wrinkle domains. Indeed, while $\sigma_{\rm L}$ is not the true stress in the shell (and neither is $\varepsilon_{\rm eff}$ the true strain), knowledge of it reveals constraints on the patterns to the point that it is an order parameter for wrinkle domains.

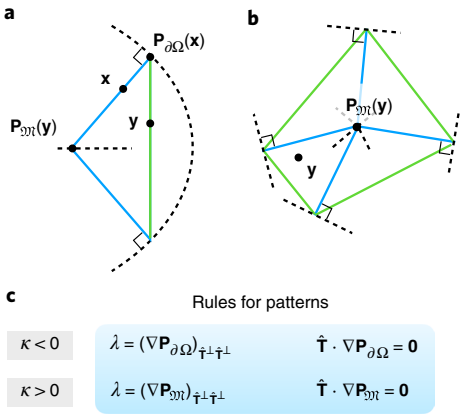

Fig. 5 | Deducing the simple rules. a,**b**, Two geometric operations take a point $\mathbf{x}$ in the shell's planform Ω to its closest boundary point $\mathbf{P}_{\partial\Omega}(\mathbf{x})$ as in **a**, or take a point $\mathbf{y}$ in Ω to a point $\mathbf{P}_{\mathfrak{M}}(\mathbf{y})$ on the medial axis whose closest boundary points have $\mathbf{y}$ in their convex hull (the green segment in **a** or the green polygon in **b**). Blue segments show paths of quickest exit from the medial axis $\mathfrak{M}$ to the boundary $\partial\Omega$ in dotted black. **c**, The fields λ and $\hat{\mathbf{T}}$ governing wrinkle patterns depend on the shell through these operations and the sign of its initial Gaussian curvature κ.

To explain this last remark further, note first that $\varepsilon_{\rm eff}$ cannot vanish identically in a region where the initial Gaussian curvature $\kappa(\mathbf{x})$ is nonzero. It follows from equation (5) that the rank of $\sigma_{\rm L}$ is at most one, that is,

$$\sigma_{\rm L} = \lambda\hat{\mathbf{T}}\otimes\hat{\mathbf{T}} \tag{6}$$

for some scalar and unit vector fields $\lambda(\mathbf{x})\geq 0$ and $\hat{\mathbf{T}}(\mathbf{x})$, where $(\hat{\mathbf{T}}\otimes\hat{\mathbf{T}})_{ij}=\hat{T}_i\hat{T}_j$. These fields contain information about the patterns. In particular, by equations (5) and (6),

$$\lambda(\varepsilon_{\rm eff})_{\hat{\mathbf{T}}\hat{\mathbf{T}}} = 0. \tag{7}$$

In regions where $\lambda>0$, the $\hat{\mathbf{T}}\hat{\mathbf{T}}$ component of $\varepsilon_{\rm eff}$ must vanish, indicating an ordered domain with wrinkle peaks and troughs along $\hat{\mathbf{T}}$. Conversely, where $\lambda=0$, the wrinkle direction is unconstrained, permitting a disordered response. The type and layout of a given shell's wrinkle domains are predicted by its locking stress.

Remarkably, it is possible to find the locking stress of a shell without first determining its effective strain, an observation that leads to a complete derivation of our simple rules. Eliminating $\mathbf{u}_{\rm eff}$ from the Lagrangian in equation (4) by minimization yields a separate, 'dual' variational principle for $\sigma_{\rm L}$ (equation (10)). We solve it exactly in the Supplementary Information, using convex Airy potentials and an inspired application of the Legendre transform. The resulting solution formulas determine λ and $\hat{\mathbf{T}}$ by one of two basic geometric operations (Fig. 5). These formulas apply whenever the shell has no holes and if its initial Gaussian curvature $\kappa(\mathbf{x})$ is of one sign. They are the basis of our simple rules (compare Figs. 2 and 5). For instance, the fact that $\hat{\mathbf{T}}\cdot\nabla\mathbf{P}_{\partial\Omega}=\mathbf{0}$ if $\kappa<0$ explains why the wrinkles of negatively curved shells lie along directions of quickest exit to the shell boundary. The remaining rules are derived in the Supplementary Information.

Coming back to our experiments and simulations, we now derive their patterns. In Fig. 3, cyan lines are drawn along the solved-for $\hat{\mathbf{T}}$ in the predicted ordered regions (where $\lambda>0$). Each negatively curved shell is found to be completely ordered. Regions consistent with disorder (where $\lambda=0$) exist for generic positively

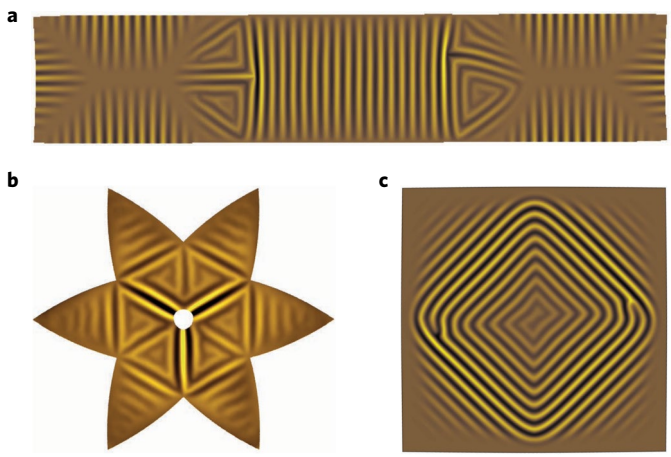

Fig. 6 | Open questions. a,**b**, While the locking stress can be defined for shells with mixed curvature ($\kappa<0$ on the left and right, $\kappa>0$ in the middle) (**a**) and shells with holes ($\kappa>0$ here) (**b**), we lack solution formulas for it in such cases. **c**, Another question regards the presence of order in regions consistent with disorder (cf. Fig. 1b).

curved shells, and are shown as polygons bordered in white. The wrinkle domains are set by the shells' medial axes following our simple rules.

Discussion. Given the success of our rules in capturing the wrinkles of confined shells, it is natural to consider other instances of reciprocity as well as graphical methods in mechanics more broadly. A well-known method is due to Maxwell[37] and also Taylor, whose reciprocal diagrams of forces and frames encode an elegant test of equilibrium for planar structures[38]. Our relations connecting the wrinkles of positively and negatively curved shells reveal a new class of reciprocal rules governing incompatible confinement. We wonder how far they generalize. Examples of shells for which we presently lack rules are shown in Fig. 6a,b. Finally, Fig. 6c highlights the fact that ordered wrinkles sometimes occur in regions the theory predicts to be consistent with disorder. Empirically, the presence of order versus disorder looks to depend on the finite wrinkle wavelength. Related to this is the question of the greatest parameter regime in which the maximum coverage problem in equation (3) can be derived. Although it predicts the patterns in our simulations and experiments well, it has yet to be established for the parameter range they explore. We imagine that a full proof of equation (3) will come from combining the 'inverted tension field theory' of ref. [19] with the ansatz-free arguments in ref. [35].

We have shown how to predict the wrinkles of confined shallow shells, using a compact set of geometric rules obtained by solving the coarse-grained theory of ref. [35]. Our results point towards a general, diagrammatic method for benchmarking elastic patterns, which could prove useful for their rapid design. We highlight a promising connection with the theory of ideal locking materials, that is, bulk materials whose microstructures facilitate extension with negligible elastic stress below a threshold strain[39]. This limit is apparently approached in biology, by the mesentery membrane of rabbits[40,41] and the capture silk of some spiders, the latter of which has recently inspired ultra-stretchable wicked membranes[42,43]. We view the wrinkles of confined shells as an emergent yet sacrificial microstructure enabling shape change. This underlies our terming the Lagrange multiplier σ_L from our solutions as the locking stress. It plays the role of an order parameter for predicting wrinkle domains. The extension of our rules beyond shallow shells and to patterns involving elements others than wrinkles, including crumples[9,44] and folds[45–47], remains to be seen.

Online content

Any methods, additional references, Nature Research reporting summaries, source data, extended data, supplementary information, acknowledgements, peer review information; details of author contributions and competing interests; and statements of data and code availability are available at https://doi.org/10.1038/s41567-022-01672-2.

Received: 9 March 2021; Accepted: 13 June 2022;
Published online: 25 August 2022

References

1. Sharon, E., Roman, B., Marder, M., Shin, G.-S. & Swinney, H. L. Buckling cascades in free sheets. *Nature* **419**, 579–579 (2002).
2. Cerda, E. & Mahadevan, L. Geometry and physics of wrinkling. *Phys. Rev. Lett.* **90**, 074302 (2003).
3. Audoly, B. & Pomeau, Y. *Elasticity and Geometry: from Hair Curls to the Non-linear Response of Shells* (Oxford Univ. Press, 2010)
4. Shyer, A. E. et al. Villification: how the gut gets its villi. *Science* **342**, 212–218 (2013).
5. Gemmer, J., Sharon, E., Shearman, T. & Venkataramani, S. C. Isometric immersions, energy minimization and self-similar buckling in non-Euclidean elastic sheets. *EPL* **114**, 24003 (2016).
6. Xu, F., Fu, C. & Yang, Y. Water affects morphogenesis of growing aquatic plant leaves. *Phys. Rev. Lett.* **124**, 038003 (2020).
7. Fei, C. et al. Nonuniform growth and surface friction determine bacterial biofilm morphology on soft substrates. *Proc. Natl Acad. Sci. USA* **117**, 7622–7632 (2020).
8. Hure, J., Roman, B. & Bico, J. Stamping and wrinkling of elastic plates. *Phys. Rev. Lett.* **109**, 054302 (2012).
9. King, H., Schroll, R. D., Davidovitch, B. & Menon, N. Elastic sheet on a liquid drop reveals wrinkling and crumpling as distinct symmetry-breaking instabilities. *Proc. Natl Acad. Sci. USA* **109**, 9716–9720 (2012).
10. Paulsen, J. D. Wrapping liquids, solids, and gases in thin sheets. *Annu. Rev. Condens. Matter Phys.* **10**, 431–450 (2019).
11. Vella, D. Buffering by buckling as a route for elastic deformation. *Nat. Rev. Phys.* **1**, 425–436 (2019).
12. Timounay, Y. et al. Sculpting liquids with ultrathin shells. *Phys. Rev. Lett.* **127**, 108002 (2021).
13. Breid, D. & Crosby, A. J. Curvature-controlled wrinkle morphologies. *Soft Matter* **9**, 3624–3630 (2013).
14. Stoop, N., Lagrange, R., Terwagne, D., Reis, P. M. & Dunkel, J. Curvature-induced symmetry breaking determines elastic surface patterns. *Nat. Mater.* **14**, 337–342 (2015).
15. Reis, P. M. A perspective on the revival of structural (in)stability with novel opportunities for function: from buckliphobia to buckliphilia. *J. Appl. Mech.* **82**, 111001 (2015).
16. Aharoni, H. et al. The smectic order of wrinkles. *Nat. Commun.* **8**, 15809 (2017).
17. Bella, P. & Kohn, R. V. Wrinkling of a thin circular sheet bonded to a spherical substrate. *Philos. Trans. R. Soc. A* **375**, 20160157 (2017).
18. Zhang, X., Mather, P. T., Bowick, M. J. & Zhang, T. Non-uniform curvature and anisotropic deformation control wrinkling patterns on tori. *Soft Matter* **15**, 5204–5210 (2019).
19. Davidovitch, B., Sun, Y. & Grason, G. M. Geometrically incompatible confinement of solids. *Proc. Natl Acad. Sci. USA* **116**, 1483–1488 (2019).
20. Tovkach, O. et al. Mesoscale structure of wrinkle patterns and defect-proliferated liquid crystalline phases. *Proc. Natl Acad. Sci. USA* **117**, 3938–3943 (2020).
21. Pretzl, M. et al. A lithography-free pathway for chemical microstructuring of macromolecules from aqueous solution based on wrinkling. *Langmuir* **24**, 12748–12753 (2008).
22. Yang, S., Khare, K. & Lin, P.-C. Harnessing surface wrinkle patterns in soft matter. *Adv. Funct. Mater.* **20**, 2550–2564 (2010).
23. Chen, C.-M. & Yang, S. Wrinkling instabilities in polymer films and their applications. *Polym. Int.* **61**, 1041–1047 (2012).
24. Li, Z. et al. Harnessing surface wrinkling–cracking patterns for tunable optical transmittance. *Adv. Opt. Mater.* **5**, 1–7 (2017).
25. Wagner, H. Ebene blechwandträger mit sehr dünnem stegblech. *Z. Flugtech. Motorluftschiffahrt* **20**, 200 (1929).
26. Pipkin, A. C. The relaxed energy density for isotropic elastic membranes. *IMA J. Appl. Math.* **36**, 85–99 (1986).
27. Steigmann, D. J. Tension-field theory. *Proc. R. Soc. Lond. Ser. A* **429**, 141–173 (1990).
28. Davidovitch, B., Schroll, R. D., Vella, D., Adda-Bedia, M. & Cerda, E. A. Prototypical model for tensional wrinkling in thin sheets. *Proc. Natl Acad. Sci. USA* **108**, 18227–18232 (2011).

29. Bella, P. & Kohn, R. V. Wrinkles as the result of compressive stresses in an annular thin film. *Commun. Pure Appl. Math.* **67**, 693–747 (2014).
30. Hohlfeld, E. & Davidovitch, B. Sheet on a deformable sphere: wrinkle patterns suppress curvature-induced delamination. *Phys. Rev. E* **91**, 012407 (2015).
31. Vella, D., Huang, J., Menon, N., Russell, T. P. & Davidovitch, B. Indentation of ultrathin elastic films and the emergence of asymptotic isometry. *Phys. Rev. Lett.* **114**, 014301 (2015).
32. Taffetani, M. & Vella, D. Regimes of wrinkling in pressurized elastic shells. *Philos. Trans. R. Soc. A* **375**, 20160330 (2017).
33. Amar, MartineBen & Jia, F. Anisotropic growth shapes intestinal tissues during embryogenesis. *Proc. Natl Acad. Sci. USA* **110**, 10525–10530 (2013).
34. van Rees, W. M., Vouga, E. & Mahadevan, L. Growth patterns for shape-shifting elastic bilayers. *Proc. Natl Acad. Sci. USA* **114**, 11597–11602 (2017).
35. Tobasco, I. Curvature-driven wrinkling of thin elastic shells. *Arch. Ration. Mech. Anal.* **239**, 1211–1325 (2021).
36. Ciarlet, P. G. *Mathematical Elasticity. Vol. II*, *Studies in Mathematics and its Applications*, *Vol. 27* (North-Holland, 1997).
37. Maxwell, J. C. XLV. On reciprocal figures and diagrams of forces. *Philos. Mag.* **27**, 250–261 (1864).
38. S. P., Timoshenko, *History of Strength of Materials. With a Brief Account of the History of Theory of Elasticity and Theory of Structures* (McGraw-Hill Book Company, 1953).
39. Prager, W. On ideal locking materials. *Trans. Soc. Rheol.* **1**, 169–175 (1957).
40. Fung, Y. C. Elasticity of soft tissues in simple elongation. *Am. J. Physiol.* **213**, 1532–1544 (1967).
41. Prager, W. On the formulation of constitutive equations for living soft tissues. *Q. Appl. Math.* **27**, 128–132 (1969).
42. Elettro, H., Neukirch, S., Vollrath, F. & Antkowiak, A. In-drop capillary spooling of spider capture thread inspires hybrid fibers with mixed solid–liquid mechanical properties. *Proc. Natl Acad. Sci. USA* **113**, 6143–6147 (2016).
43. Grandgeorge, P. et al. Capillarity-induced folds fuel extreme shape changes in thin wicked membranes. *Science* **360**, 296–299 (2018).
44. Timounay, Y. et al. Crumples as a generic stress-focusing instability in confined sheets. *Phys. Rev. X* **10**, 021008 (2020).
45. Pocivavsek, L. et al. Stress and fold localization in thin elastic membranes. *Science* **320**, 912–916 (2008).
46. Brau, F., Damman, P., Diamant, H. & Witten, T. A. Wrinkle to fold transition: influence of the substrate response. *Soft Matter* **9**, 8177–8186 (2013).
47. Paulsen, J. D. et al. Geometry-driven folding of a floating annular sheet. *Phys. Rev. Lett.* **118**, 048004 (2017).

Methods

Experiment. Dilute solutions of polystyrene ($M_n = 99$ kDa, $M_w = 105.5$ kDa; Polymer Source) in toluene (99.9%; Fisher Scientific) were spin-coated onto glass substrates of various positive and negative Gaussian curvatures. The positively curved substrates were spherical optical lenses (Thorlabs, Inc.). Negatively curved shells were formed on a single negative-curvature substrate that is less controlled by comparison. Its principal radii of curvature were measured from side-view images and are reported in Supplementary Table S1.

The film thickness was varied by changing the polymer concentration and spinning speed. Different shapes were cut out using a metal scribe. After preparing the glass substrates with a thin layer of poly(acrylic acid), the films were released by dissolving this sacrificial layer in water. The films were finally transferred to a pure water–air interface. Following the experiments, each film was captured and its thickness measured using a white-light interferometer (Filmetrics F3).

The shells were shallow with $0.01 < (W/R)^2 < 0.2$ and have nondimensional bending modulus $b = BR^2/YW^4$ in the range $4\times10^{-11} < b < 2\times10^{-8}$. The nondimensional substrate stiffness $k = KR^2/Y$ and nondimensional surface tension $\gamma = \gamma_{lv}R^2/YW^2$ obey $0.003 < k < 0.03$ and $4\times10^{-4} < \gamma < 10^{-2}$. Additionally, $10^{-2} < \gamma/k < 0.7$, $10^{-6} < 2\sqrt{bk} < 3\times10^{-5}$ and $10^{-3} < (b/k)^{1/4} < 10^{-1}$. These ranges are in line with all but one of the assumptions used in ref. [35] to derive equation (2) (not obeying $(b/k)^{1/10} \ll \gamma + 2\sqrt{bk}$). Specific parameters for the experiments shown in the main text are presented in Supplementary Tables S1 and S2.

Simulation. Shells bonded to a planar liquid substrate without surface tension were simulated in the finite element package ABAQUS/Explicit. Four-node thin shell elements with reduced integration (element type S4R) were used. The confining force was specified as a nonuniform distributed pressure load over the surface of the shell, via a VDLOAD subroutine. Otherwise, free boundary conditions were used. Comparative nonlinear geometric finite element analysis using linearly elastic and neo-Hookean hyperelastic materials showed that the results are largely independent of the model. Colour coding in the images corresponds to vertical deflection from the plane.

In the same nondimensional groups as before, the simulations have $0.01 < (W/R)^2 < 0.04$, $7\times10^{-9} < b < 2\times10^{-6}$, $6 < k < 40$ and $\gamma = 0$. Additionally, $2\times10^{-4} < 2\sqrt{bk} < 2\times10^{-2}$ and $5.6\times10^{-3} < (b/k)^{1/4} < 10^{-2}$. As with the experiments, these ranges are in line with all but one of the assumptions of ref. [35] (not obeying $(b/k)^{1/10} \ll 2\sqrt{bk}$). Specific parameters for the simulations shown in the main text are presented in Supplementary Table S3.

Theory. Here we connect the Lagrangian $\mathcal{L}$ in equation (4) to our coarse-grained fields. We assert the existence of a saddle point $(\mathbf{u}_{\text{eff}}, \sigma_{\text{L}})$ satisfying

$$\mathcal{L}\{\mathbf{u}_{\text{eff}} + \delta\mathbf{u}_{\text{eff}}, \sigma_{\text{L}}\} \geq \mathcal{L}\{\mathbf{u}_{\text{eff}}, \sigma_{\text{L}}\} \geq \mathcal{L}\{\mathbf{u}_{\text{eff}}, \sigma_{\text{L}} + \delta\sigma_{\text{L}}\} \tag{8}$$

for all $\delta\mathbf{u}_{\text{eff}}$ and $\delta\sigma_{\text{L}}$ with $\sigma_{\text{L}} + \delta\sigma_{\text{L}} \geq 0$ (see ref. [35]). The key linking saddle points to the maximum coverage problem (equation (3)) is that such points yield its solutions. To study saddles in detail, we evaluate the min–max and max–min procedures $\min_{\mathbf{u}_{\text{eff}}} \max_{\sigma_{\text{L}}} \mathcal{L}$ and $\max_{\sigma_{\text{L}}} \min_{\mathbf{u}_{\text{eff}}} \mathcal{L}$.

First, consider the min–max. We claim that

$$\min_{\mathbf{u}_{\text{eff}}} \max_{\sigma_{\text{L}}} \mathcal{L} = \min_{\mathbf{u}_{\text{eff}}} \Delta A, \tag{9}$$

where on the right the tension-free constraint $\varepsilon_{\text{eff}} \leq 0$ is used. Equation (9) states that solving the maximum coverage problem is equivalent to finding the min–max of $\mathcal{L}$ and explains why its saddle points contain our effective displacements. To prove this, note that the inner maximization over $\sigma_{\text{L}} \geq 0$ enforces the tension-free constraint. Indeed, if a component of ε_{eff} is positive, then by sending the same component of σ_{L} to infinity, we obtain $\max \mathcal{L} = \infty$, while conversely, if $\mathbf{u}_{\text{eff}}$ is tension free, then $\int_\Omega \sigma_{\text{L}} : \varepsilon_{\text{eff}} \leq 0$ and $\max \mathcal{L} = \Delta A$. Evidently, minimizing the maximum prefers tension-free states. It follows that saddle points achieve $\mathcal{L} = \Delta A$ or, equivalently, that $\int_\Omega \sigma_{\text{L}} : \varepsilon_{\text{eff}} = 0$. Since the integrand is nonpositive, it must vanish, proving the orthogonality relation in equation (5).

Next, consider the max–min. A computation in the Supplementary Information using the divergence theorem gives

$$\max_{\sigma_{\text{L}}} \min_{\mathbf{u}_{\text{eff}}} \mathcal{L} = \max_{\sigma_{\text{L}}} -\frac{1}{2}\int_{\mathbb{R}^2} \nabla p \otimes \nabla p : (\sigma_{\text{L}} - I), \tag{10}$$

where in the resulting maximization σ_{L} is constrained to be a nonnegative symmetric matrix-valued field equalling the identity I exterior to Ω and that is weakly divergence free on $\mathbb{R}^2$. This is the dual problem mentioned in the main text, and solving it gives the locking stress associated with Ω and p. The choice to extend σ_{L} beyond the shell relaxes its boundary conditions so that a maximizer always exists[35]. The original boundary condition $\sigma_{\text{L}}\hat{\mathbf{n}} = \hat{\mathbf{n}}$ can be thought of as happening outside of an infinitesimally thin boundary layer at $\partial\Omega$. The inner boundary values of σ_{L} can then be optimized. This relaxation is crucial to capturing the patterns of positively curved shells (Fig. 3). The dual problem for σ_{L} is discussed further in the Supplementary Information, where we solve it using convex Airy potentials to derive our simple rules.

Data availability

The parameters for the shells in Figs. 1–4 are presented in Supplementary Tables S1–S3. Dimensionless parameter ranges for the experiments and simulations are given in Methods. Individual parameters for all experiments are also provided as a Supplementary Datafile. All other data that support the findings of this study are available from the corresponding authors upon reasonable request.

Acknowledgements

We thank B. Davidovitch, V. Démery, C. R. Doering, G. Francfort, S. Hilgenfeldt, R. D. James, R. V. Kohn, N. Menon, P. Plucinsky, D. Vella and A. Waas for helpful discussions. This work was supported by NSF awards DMS-1812831 and DMS-2025000 (I.T.); NSF award DMR-CAREER-1654102 (Y.T., J.D.P.); NSF award PHY-CAREER-1554887, University of Pennsylvania MRSEC award DMR-1720530 and CEMB award CMMI-1548571, and a Simons Foundation award 568888 (D.T. and E.K.).

Author contributions

I.T., E.K. and J.D.P. conceived and designed the research. I.T. developed and implemented the theory. D.T. and E.K. conducted and analysed the simulations. Y.T., G.C.L. and J.D.P. conducted and analysed the experiments. I.T., Y.T., D.T., E.K. and J.D.P. wrote the manuscript.

Competing interests

The authors declare no competing interests.

Additional information

Supplementary information The online version contains supplementary material available at https://doi.org/10.1038/s41567-022-01672-2.

Correspondence and requests for materials should be addressed to Ian Tobasco, Joseph D. Paulsen or Eleni Katifori.

Peer review information *Nature Physics* thanks Enrique Cerda and the other, anonymous, reviewer(s) for their contribution to the peer review of this work.